USSR ACADEMY OF SCIENCES
A.F. IOFFE ORDER OF LENIN PHYSICO-TECHNICAL INSTITUTE, LENINGRAD

Report 430

INVESTIGATION OF ELASTIC pp-SCATTERING IN THE COULOMB INTERFERENCE REGION IN THE ENERGY RANGE 500-1000 MeV

A.A. Vorob'ev, A.S. Denisov, Yu.K. Zalite, G.A. Korolev,
V.A. Korolev, G.G. Kovshevnyj, E.M. Maev, V.I. Medvedev,
G.L. Sokolov, G.E. Solyakin, E.M. Spiridenkov,
I.I. Tkach and V.A. Shchegel'skij

Leningrad 1972

Translated at CERN by R. Luther
(Original: Russian)
Not revised by the Translation Service

(CERN Trans. Int. 73-1)

Geneva
January 1973

Using a pulsed ionization chamber filled with hydrogen to record the recoil protons, the differential cross-sections of elastic pp-scattering are measured in the momentum transfer region $2 \cdot 10^{-3} \leqslant |t| \leqslant 8 \cdot 10^{-3}$ $(GeV/c)^2$. The measurements are carried out at $P_{lab.}$ = 1.11 GeV/c, 1.28 GeV/c, 1.34 GeV/c, 1.40 GeV/c and 1.70 GeV/c. The real part of the spin-independent amplitude of the pp-interaction is determined. The results are in agreement with the dispersion relation calculations.

By investigating the differential cross-section of elastic hadron scattering in the interference region of Coulomb and nuclear interactions, the real part of the spin-independent amplitude of forward scattering Re A_{ns} (0) may be calculated. This value may also be calculated by means of dispersion relations. Hitherto experimental results have mostly been in agreement with the dispersion relation forecasts, the exception being data on proton-proton scattering in the energy range 600-800 MeV. The experimental values of α = Re $A_{ns}(0)$/ Im A_{ns} (0) obtained in the reports by Dutton et al.[1,2], differ markedly from the theoretical forecasts. For example, at 650 MeV $\alpha_{exp.} = - 0.76 \pm 0.13$ whilst $\alpha_{theor.} = + 0.3$.

This report includes the results of an investigation into elastic pp-scattering at $P_{lab.}$ = 1.1 - 1.7 GeV/c in the momentum transfer region $2 \cdot 10^{-3} \leqslant |t| \leqslant 8 \cdot 10^{-3}$ $(GeV/c)^2$.

METHOD

The measurements were carried out using a new method for detecting recoil protons based on an ionization chamber filled with hydrogen (fig. 1). The chamber acts both as a gas target and as a detector of recoil protons. By measuring the shape of the signals on the chamber's electrodes and the signals' delay time in relation to the moment when a scattered particle passes through the chamber, the energy T_p and the emission angle ϑ of the recoil proton may be determined, and the gas target's volume may be defined inside the

chamber's useful volume. The energy T_p is determined by the pulse height at the central anode V_a (or by the sum of the pulse heights at the central anode V_a and orifice anode V_{ka} if the proton's path is longer than the anode's radius but shorter than the external radius of the orifice). The angle φ is determined by the pulse's leading edge at the central anode. By measuring the time interval $t_a - t_o$, the distance from the grid to the nearest end of the track may be determined (t_o is the instant when the proton passes through, determined by scintillation counters, and t_a is the instant when a pulse occurs at the anode). By analyzing the signals from the chamber, particles occuring in the electrodes (or behind the electrodes) and remaining in the chamber's useful volume may be excluded. Background reactions occuring in the gas target are also eliminated - namely elastic scattering with a large momentum transfer and inelastic scattering accompanied by the production of mesons. The number of particles passing through the chamber is determined by a direct count using a telescope of scintillation counters $S_1\hat{S}_2\hat{S}_3$, operating in coincidence with the pulse from the V_k cathode. By controlling the chamber in this way, it is possible to reduce considerably the background of nuclear reactions and the background caused by neutron scattering in the chamber's sensitive volume. Check measurements showed that the efficiency of counter S_3 was independent with up to 0.2% accuracy of the point where the proton struck the crystal. Pulses occuring at the chamber's electrodes due to the passage of primary protons are relatively low in value (20 - 40 keV). Moreover, they are compensated by a special circuit triggered from the scintillation counters $S_1\hat{S}_2$. A more detailed description of the method and also of the results of an investigation into the ionizing properties of hydrogen (recombination, adhesion, diffusion, electron mobility, energy-ionization dependence) will be given in a later article. We shall give only a list of the chamber's main parameters for this experiment.

Measured energy range of the recoil protons -

$$1.0 \text{ MeV} \leqslant T_p \leqslant 4.0 \text{ MeV}.$$

Energy resolution FWHM $\simeq$ 40 keV.

Error in defining the thickness of the gas target - 2%.

Electron drift time from cathode to grid - 17 /usec.
from grid to anode - 2 /usec.
Time resolution FWHM = 0.3 - 0.5 /usec.
Angular resolution $\Delta\varphi$ = 0.5° - 5°.
Maximum permissible intensity of continuous beam - $2 \cdot 10^4$ protons/sec.
Data acquisition rate at $\sigma_{tot.}$ = 40 mbarn and $I_p = 10^4$ protons/sec. - 120 useful events per hour.

ELECTRONICS SYSTEM

The electronics system for the experiment consists of spectrometric channels, a system for the analog selection of events, a counter system, a control system and a system for collecting and storing data. A block diagram of the device and a time diagram of the pulses are shown in Fig. 2 and Fig. 3 respectively.

Signals generated at the chamber's electrodes and amplified by the preamplifiers PA are transmitted to the amplifiers A1 - A4 and shapers Sh4 and Sh5. The output signals from the amplifiers and converters C1 and C2 were transmitted to the amplitude storage units. These units served as an intermediate analog store during the selection of events. Moreover, they standardized the signals for the amplitude-digital code converters.

The trigger signal (event, fig. 3) is a pulse from the triple coincidence circuit (CC2) which determines the moment when a proton passes through the chamber. The shaper Sh4 shapes a 4 /usec pulse when a recoil proton is formed. The coincidence (CC3) of this pulse with the trigger signal which passed through the protection and delay unit (PDU3) is the start signal for the event recording system. The protection unit (PDU3) selects an event only if no proton is recorded during the 4 /usec before or after the event. The control unit (CO-001) shapes the "gate" covering the possible delay range for the signal from the chamber's anode, opens the Sh5 shaper's input and interlocks the shapers in the trigger system Sh1-Sh3. At

the end of the gate, a check is made to see whether there is a test signal from Sh5. If there is a signal, the event recording system is triggered: the output voltage from the pulse height storage units (PHSU 1-6) is gated to the amplitude-digital converter system VIST[3] and as the coding is completed a call is transmitted to the data acquisition system SONIK[4]. If the signal from Sh5 is not received within a given time, the temporary store is discarded and the selection system unlocked. The trigger signal is the start signal for the time-amplitude converters C1 and C2 which measure the distribution of events in the time window (C1) and over the chamber volume (C2). The pulses from Sh4 and Sh5 are stop signals. As the Sh4 shaper has a high level of noise activity due to its low threshold, the C2 converter has a start protection circuit (CC3 and distributor D). The event selection circuits are opened by a timer synchronized with the beam in order to avoid any overloading of the system when ejection starts. In order to check the event distribution against the beam duration, the moment when the event occured was recorded in relation to the start of the beam. A linear function voltage generator (LFVG) synchronized with the acceleration cycle was used for this purpose.

As the measurements had to be extremely accurate, it was necessary to use a system whereby a constant check could be kept on the parameters of the counter system, analog selection system and spectrometric system. The monitoring system included a digital precision amplitude generator (GAMBIT)[5] and a time interval generator. The voltage from the GAMBIT was proportional to the fixed code N1 (the accuracy of the volatge device was not worse than 10^{-4}) and was transmitted to the precision pulse-height shapers which were connected to the chamber's preamplifiers. According to the signals from the precise-time generator (accuracy of time interval - 0.1 /usec.), pulses were transmitted to the preamplifiers with a polarity and shape similar to those of the chamber's real signals. At the starting instant t_o the photodiodes IS1-IS3 were fired, simulating the passage of a proton; at that instant the signal reached the cathode, corresponding to the occurence of a recoil proton. At the instant t_{N2} pulses were transmitted to the anode and orifice.

The "useful event" in the chamber was thus fully simulated. The channels' stability was checked and their integral non-linearity measured using 16 stages of amplitude for the monitor signals and 8 stages of delay for the signals at the anode (orifice) in relation to the pulse at the cathode. Test events were generated throughout the experiment and the programme for amplitude and time variation was set by means of a special unit. A phasing circuit permitted the generation of a test event only when there was no useful event. By marking the test event, it was possible to identify the test data on the computer. As the test events are a complete simulation of the useful events, it is possible to test the whole system's recording efficiency. The latter was expressed as the ratio of the number of recorded test events to the number counted by the CC4 coincidence circuit. The computer stopped the measurements if efficiency dropped to $< 98\%$.

The counting system consisted of ten scaling circuits connected to a "PRINT-OUT" console (JINR development). During the experiment the counting system recorded the number of counts from S_1, S_2 and S_3, the number of double coincidences $S_1 \hat{} S_2$, the number of triple coincidences $S_1 \hat{} S_2 \hat{} S_3$, the number of triple coincidences after the protection unit $S_1 S_2 S_3$* (the number of protons recorded), the number of generator pulses recorded by the CC4 circuit and the number of CC3, Sh4 and Sh5 operations. Data from the counting system was fed into the computer via the SONIK system. By comparing the readings from the scaling circuits after each ejection cycle, it was possible to check the efficiency of the counters, the stability of the shapers' thresholds and the efficiency of the event selection system. All the information was fed into a "MINSK-22" computer and was recorded on magnetic tape after the temporary store had been filled. Control matrices and histograms were printed out periodically.

PRODUCTION OF PROTONS BEAMS

The experiment required beams of $\sim 10^4$ protons/sec. with a maximum duty cycle. A 1000 MeV low-intensity proton beam was obtained in the following way. The accelerator's frequency program was

interrupted directly before beam ejection so that the protons continued to circulate in the accelerator for some time ($\sim$ 2 sec.). Some of the protons were scattered in the residual gas, entered the regenerator region and were extracted from the accelerator. Diagrams of the beam's layout and parameters are shown in Fig.'s 4-6. Proton beams of lower energy were obtained by absorbing a part of the energy in a copper attenuator. As the intensity of the beam ejected by means of gas scattering was inadequate, the beam was extended in time by means of the Si electrode. The system for producing the beam is shown in fig. 7. Fig.'s 8 and 9 illustrate the beam's time structure and profile at 510 MeV. The average proton energy was determined by plotting path against energy in copper. Furthermore, check measurements were carried out in terms of time of flight over a distance of 31.6 m (S_o - start, S_1 - stop, fig. 7). The results are shown in table 1.

Table 1

Proton energy in the beams

Thickness of attenuator		Rated energy	Energy measured in terms of time of flight
mm.	g/cm^2*	MeV	MeV
176.0	157	750	-
209.6	187	698	714±14
242.4	216	648	650±12
326.0	291	513	-

*) ρ = 8.942±0.018 g/cm^3.

These measurements showed (fig. 10) that the admixture of other particles, deuterons in particular, in the proton beam was negligible. The beams' energy spectra could also be estimated and the value of the low-energy tail determined. Fig. 11 shows the results of the time-of-flight measurements when the start pulse was given by a frequency mark from the Si electrode's HF generator. In this case the distribution width defines the beam's microstructure rather than the energy spread. However, good background conditions permit a

reliable measurement of the distribution tail: the number of protons with $t - \bar{t} \geqslant 10$ nsec. is less than 0.1%. By combining this result with the data in fig. 10. it may be concluded that at $T_p = 510$ MeV the number of protons with $T_p \leqslant 450$ MeV does not exceed 2%.

RESULTS

Fig. 12 shows the event matrix with energy and angle as the coordinates. The test matrix together with all the one-dimensional distributions of the useful and test events were printed out periodically. During ejection it was possible to set up "windows" in the different channels. A "mode of anticoincidence with the orifice" was used ($V_{ka} \leqslant 100$ keV) and"volume" restrictions were applied: $(t_a - t_o)_{min.} < t_a - t_o < (t_a - t_o)_{max.}$. In this matrix the useful events ($\varphi \approx 90°$) must lie along the diagonal. As can be seen in fig. 12, at energy $T_p > 1.6$ MeV, there is no problem in separating useful from background events. However, as T_p decreases, the background increases. A large part of the background is caused by scattering of neutrons in the chamber's useful volume. These events are evenly distributed in the time window and may be deducted by an appropriate extrapolation. An "energy-time window" matrix was used for this purpose (fig.13). The background was deducted at several thresholds in the angular channel. The minimum energy of recoil protons used in the processing of the results was $T'_p \sim 1.25$ MeV. The value of the background deducted did not exceed 20% of the number of events. As T_p increases, the proportion of the number of background events to that of useful events drops, and at 3 MeV it is approximately 1%.

In order to find events which corresponded to a recoil proton energy range from 3 to 4 MeV, the total number of pulses from the anode and the orifice was used. Fig. 14 shows the matrix $V_a - V_{ka}$. The distribution of events has a characteristic triangular form. For tracks not exceeding the radius of the anode, the pulse height at the orifice is close to zero (induced pulses). Events for which the track length is greater than the anode's radius but less than

the outer radius of the orifice form the upper side of the triangle. They correspond to increasing V_{ka} and vanishing V_a. Finally, the third side of the triangle - vanishing V_a and V_{ka} - is composed of events, the particle track of which exceeds the outer radius of the orifice. When adding the pulse heights of the anode and orifice, 1.4% of the total height was deducted to take into account induction from one electrode to the other. The background was deducted in the same way as at the lower energies.

When calculating the differential cross-section, it is essential to know the exact dimensions of the useful volume. In order to exclude the background (reactions at the cathode and on the grid) $\sim$ 75% of the useful volume is used. This is achieved by introducing the "windows" in the channel $t_a - t_o$. The main error relates to the graduated scale of the time delay analyzer which must be accurately related to the grid-cathode distance. The position of the zero on the scale, corresponding to tracks in the grid plane, and the linearity of the scale were both checked by means of a generator. The time channel, corresponding to the track's position in the cathode plane, was determined by means of pulses from an α-source applied to the cathode. Low-energy α-particle pulses, emitted almost parallel to the electrode, were selected for this purpose. The dependence of V_k/V_a on $(t_a - t_o)$ was used as $V_k/V_a = 1$ corresponds to a track, the centre of gravity of which lies in the cathode's plane. The ratio f of the number of channels used in the time delay analyzer $(t_a - t_o)$ to the total number of channels indicates the proportion of the chamber's volume used. As this value is a factor in the formula for the differential cross-section, the accuracy of the latter depends on the accuracy with which f is determined. In our case the accuracy was $\sim$ 2%.

The energy scale was graduated in therms of the energy of the α-line ^{234}U E_α = 4.768 MeV. Using the energy-path curve of protons in hydrogen and the ratio of pulse heights from the anode and the orifice, it was shown with $\sim$ 3% accuracy that the energy used in producing a pair of ions in the ionization of α-particles and of protons is the same.

Fig's. 15-19 give the measured differential cross-sections at $P_{lab.}$ = 1.1 - 1.7 GeV/c. In order to determine the ratio, the following interference formula was used

where

$A_c = \frac{k}{137MT_p\beta_p}$ is the Coulomb scattering amplitude,

$\sigma_{tot.}$ – is the total cross-section of the pp-interaction,

M – is the proton's mass, β_p is the proton's velocity,

k is the proton's momentum , h = c = 1,

β – parameter which takes into account the contribution of spin-dependent amplitudes. The parameters α and β in table 2 were determined by the least squares method.

Table 2

Results of measurements

Protons' momentum GeV/c	$\sigma_{tot.}$ /7/ mbarn	α	β	χ^2	No. of degrees of freedom
1.11	34.03	0.321±0.074	0.274±0.065	28	27
1.28	43.23	0.294±0.073	-0.065±0.040	30	26
1.34	44.86*)	0.372±0.088	0.059±0.062	59	25
1.40	46.49	0.099±0.082	0.013±0.061	18	25
1.70	47.55	-0.105±0.085	0.008±0.086	48	43

*) Extrapolated value.

This table gives the correponding values of χ^2 . A 1000 MeV experiment was performed mainly in order to check the method as the existing experimental data /1,8/ are in agreement and do not contradict the theory of dispersion relations. The results of our measurements are also in good agreement with these data. Fig. 20 shows the theoretical values of the α-parameter calculated from dispersion relations. The Figure also gives the known experimental values of

α in the momentum range 1.1 - 1.7 GeV/c. The values that we obtained are in good agreement with the theoretical predictions and differ sharply from Dutton's data.

In conclusion, the authors wish to thank A.V. Kulikov and the staff of the Accelerator Department at the Leningrad Institute of Nuclear Physics for ensuring the operation of the synchrocyclotron in the right conditions for the experiment, and also the staff of the Radioelectronics Department of the Laboratory for High-Energy Physics for their great help in developing and preparing the apparatus and for running the experiments on-line with a computer. The authors are also grateful to V.M. Zajtsev and Yu.S. Grigor'ev for their spectrometric analysis of hydrogen and for filling the chamber, and M.F. Sobolovskij for his help in processing and formulating the results of the measurements.

****

Bibliography

1. L.M.C. Dutton, R.J.W. Howells, J.D. Jafar, H.B. van der Raay. Phys. Lett., 25B, 245 (1967).
2. L.M.C. Dutton, H.B. van der Raay. Phys. Lett., 26B, 679 (1968).
3. V.I. Kadashevich, V.I. Vinogradov, V.V. Marchenkov, A.P. Nekhaj. Preprint FTI-199, Leningrad, 1969.
4. I.I. Tkach, A.V. Kulikov, A.P. Kashchuk, N.K. Lastochkin, S.I. Kalentarova, G.A. Gorodnitskij. Preprint FTI-185, Leningrad, 1969.
5. N.K. Lastochkin, V.I. Inzhevatov, E.E. Yakovlev. PTE, 1, 109 (1971).
6. W.H. Barkas and M.J. Berger. Studies in penetration of charged particles in matter. Publication 1133. National Academy of Sciences - National Research Council, Washington, D.C., p. 103, 1964.
7. D.V. Bugg, D.C. Salter, G.H. Stafford, R.F. George, K.F. Riley, R.J. Tapper. Phys. Rev., 146, 980 (1966).
8. J.D. Dowell, R.J. Homer, Q.H. Khan, W.K. McFarlane, J.S.C. McKee, A.W. O'Dell. Phys. Lett., 12, 252 (1964).
9. V.S. Barashenkov, V.D. Toneev. JINR Preprint P2-3850, Dubna.
10. O.V. Dumbrajs. Ya.F., 5, 1096 (1971).

*****

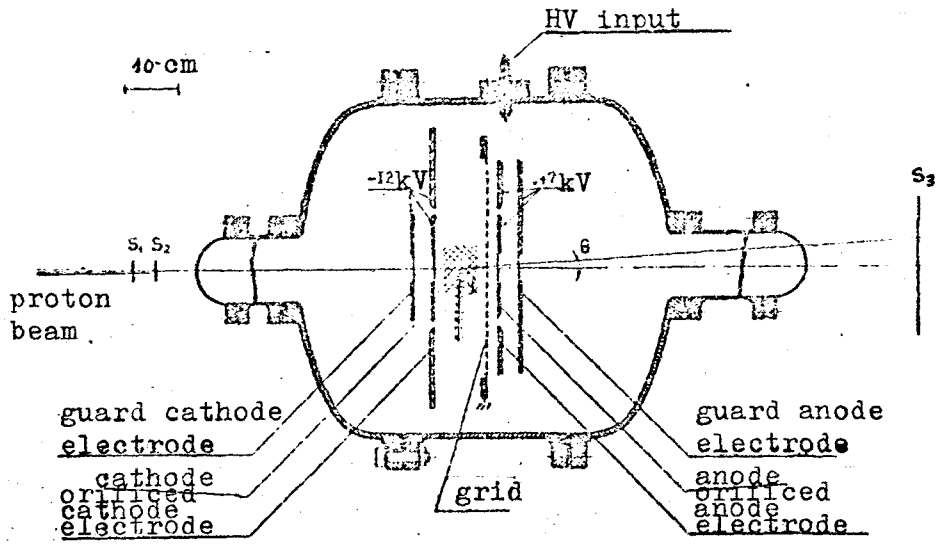

Fig. 1. Ionization chamber used to study pp-scattering at small angles.

Diameter of central electrodes 200 mm, internal diameter of orifice 220 mm, external diameter of orifice 400 mm, cathode-grid distance 100.0 - 0.2 mm, thickness of input window 0.7 mm - steel.

$S_1 S_2 S_3$ - telescope of scintillation counters.

Size of crystals S_1 and S_2 - ϕ 40 x 5,

S_3 - ϕ 250 x 10.

Hydrogen pressure in chamber 8 atm.

Content of impurities in hydrogen: $N_2 = (3\text{-}6)\cdot 10^{-3}\%$,

$O_2 \simeq 10^{-5}\%$ per volume.

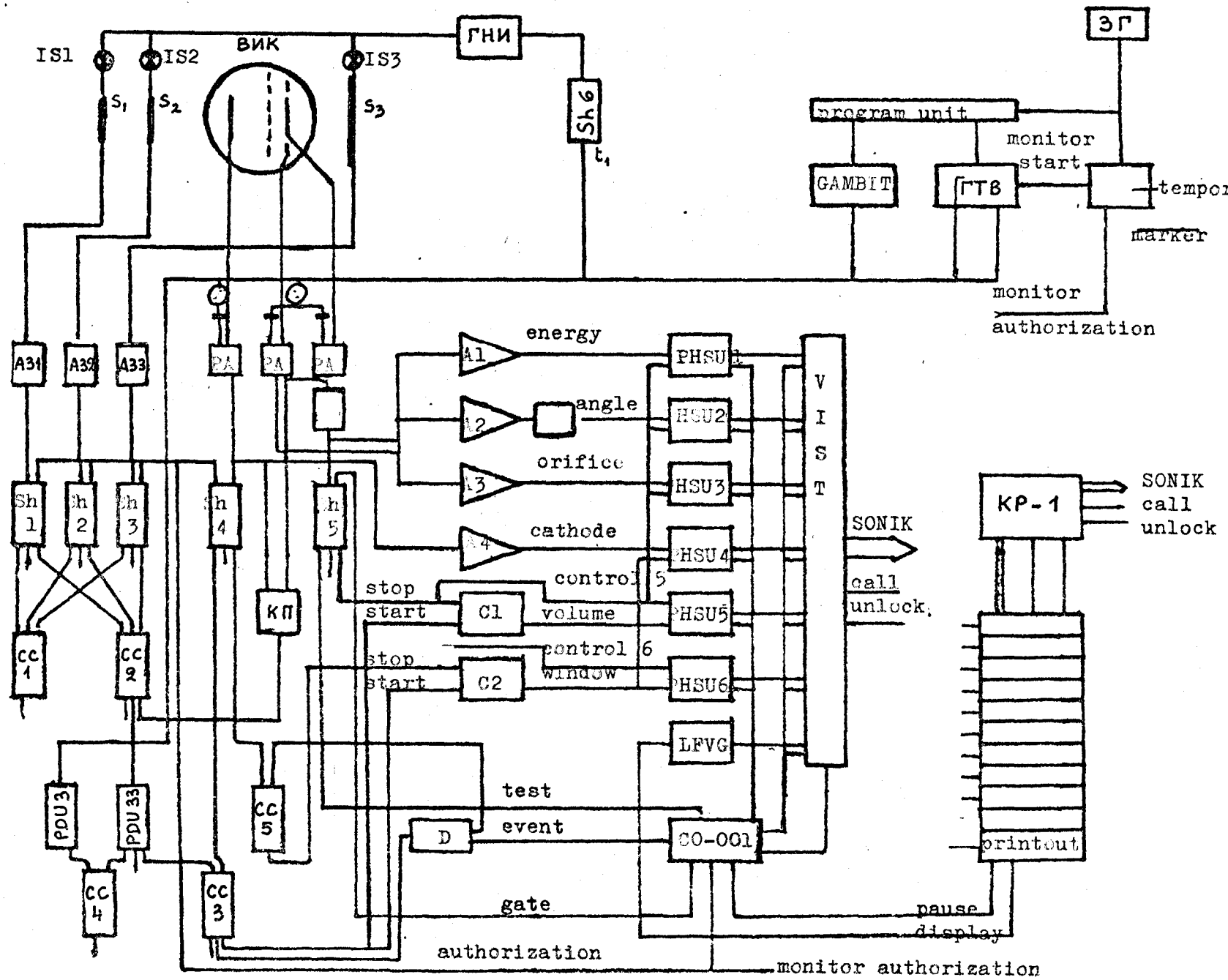

Fig. 2. Block diagram of electronics circuit.

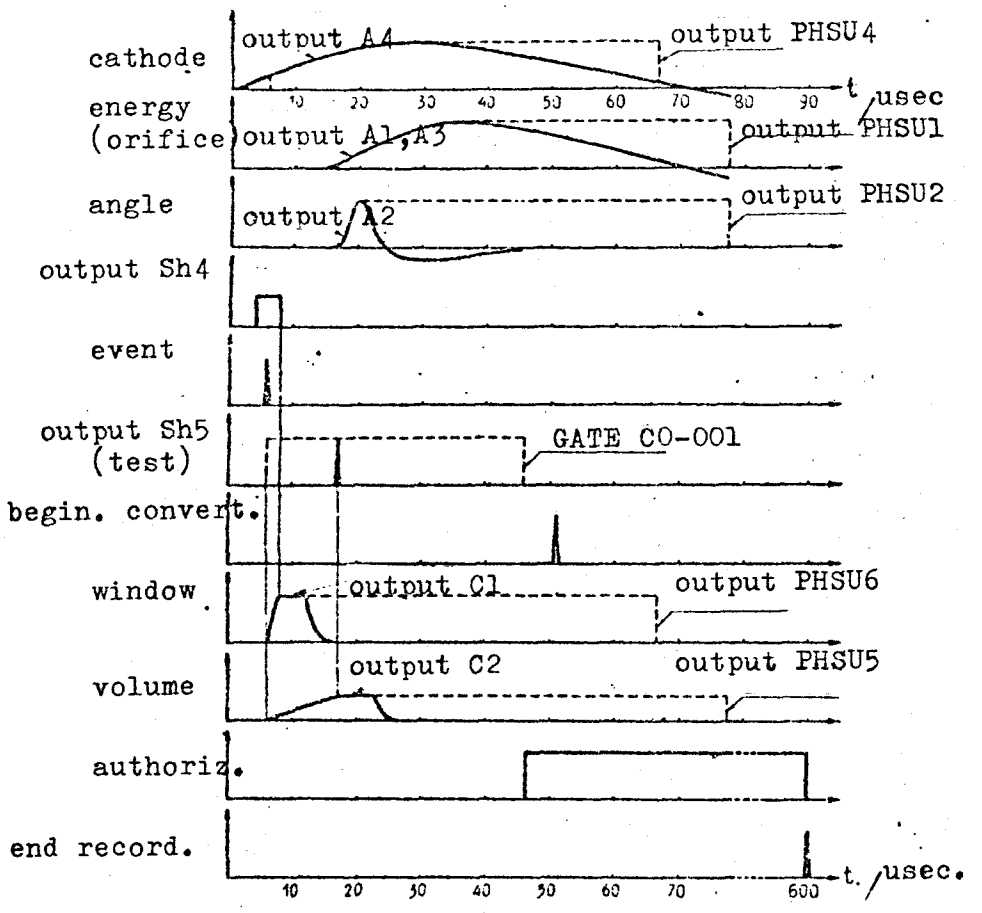

Fig. 3. Time diagram of pulses.

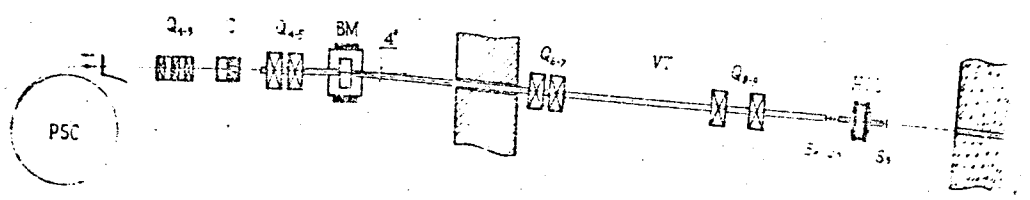

Fig. 4. Layout of experiment to measure $d\sigma_{pp}/dt$ at a proton energy of 1000 MeV.

PSC - proton synchrocyclotron
Q_{1-9} - quadrupole magnet lenses
C - collimator with adjustable slit
BM - bending magnet
VT - vacuum channel
HIC - hydrogen ionization chamber
$S_1S_2S_3$ - telescope of scintillation counters

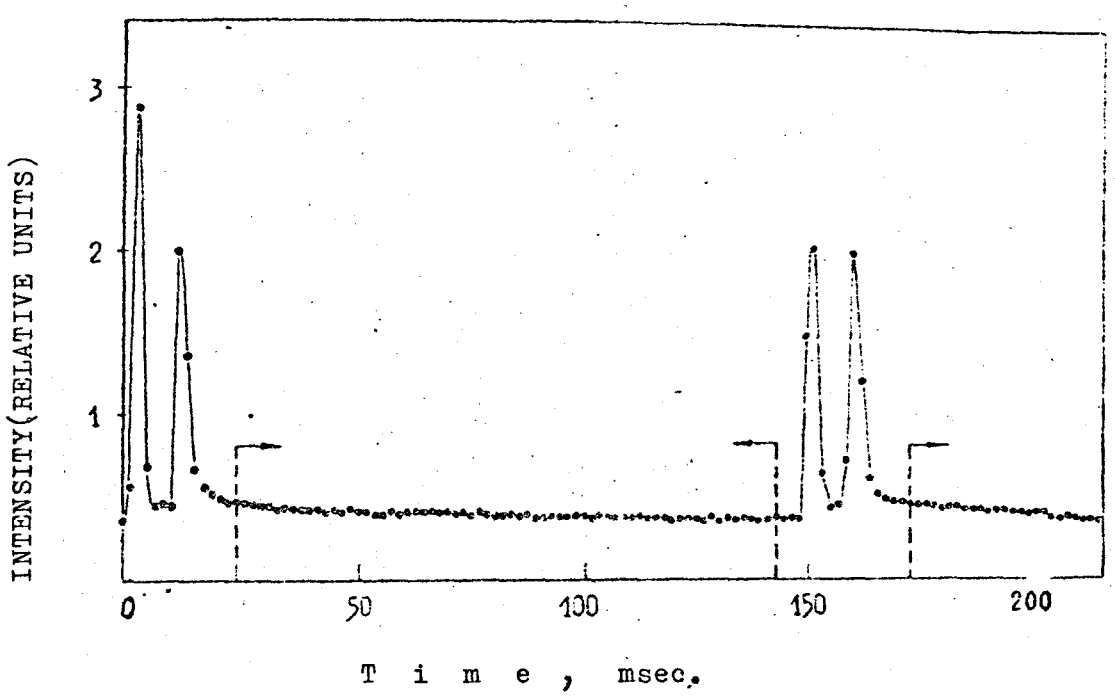

Fig. 5. Time structure of proton beam at 1000 MeV.
The beam is extracted by means of scattering on the residual gas in the accelerator chamber.
The peaks correspond to the beginning and end of acceleration.
The arrows indicate the window selected.
The beam intensity in the window $I_p = 10^4$ protons/sec.
The accelerator's frequency $f = 6^p$Hz.

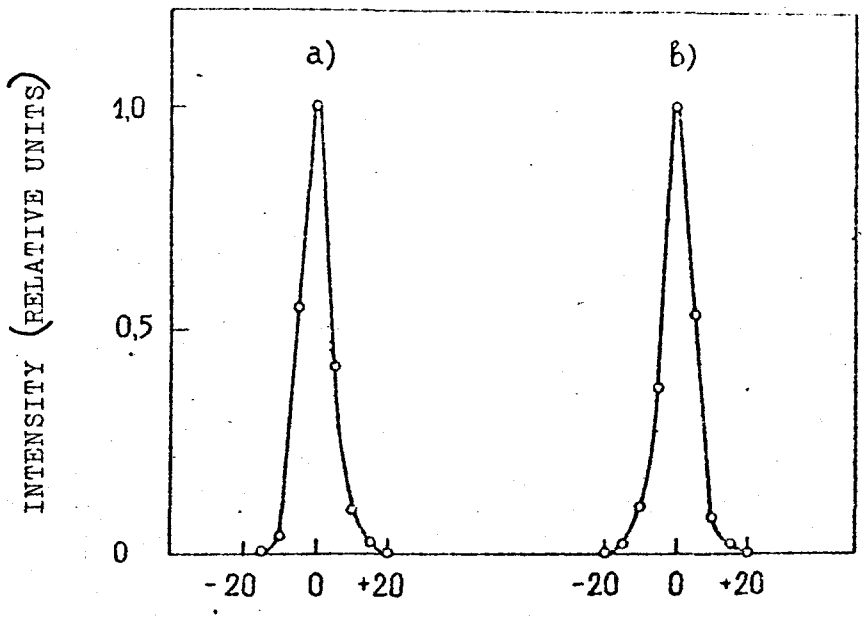

Fig. 6. Beam profile at the input to the ionization chamber.

T_p = 1000 MeV

a) - horizontal plane

b) - vertical plane

Beam spread was ± 0.3%.

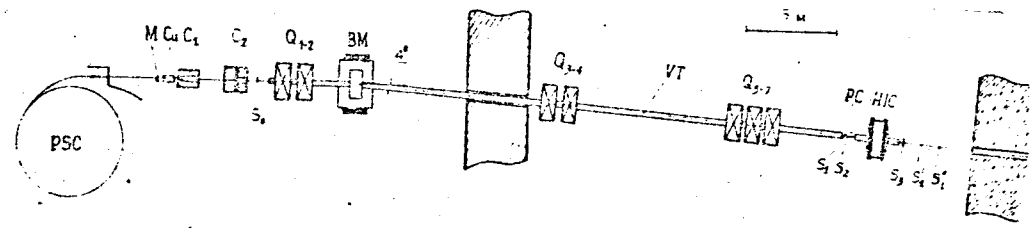

Fig. 7. Layout of experiment to measure $d\theta_{pp}/dt$ at proton energies of 750, 700, 650 and 510 MeV.

PSC - proton synchrocyclotron
M - extracted beam intensity monitor
Cu - copper attenuator
C_1 - collimator, C_2 collimator with adjustable slit
Q_{1-7} - quadrupole magnet lenses
BM - bending magnet, VT - vacuum channel
HIC - hydrogen ionization chamber
PC - proportional chamber measuring beam profile
$S_1S_2S_3$ - counter telescope
S_o-$S_1(S_1', S_1'')$ - scintillation counters used for time-of-flight analysis of the proton beam's energy spectrum.

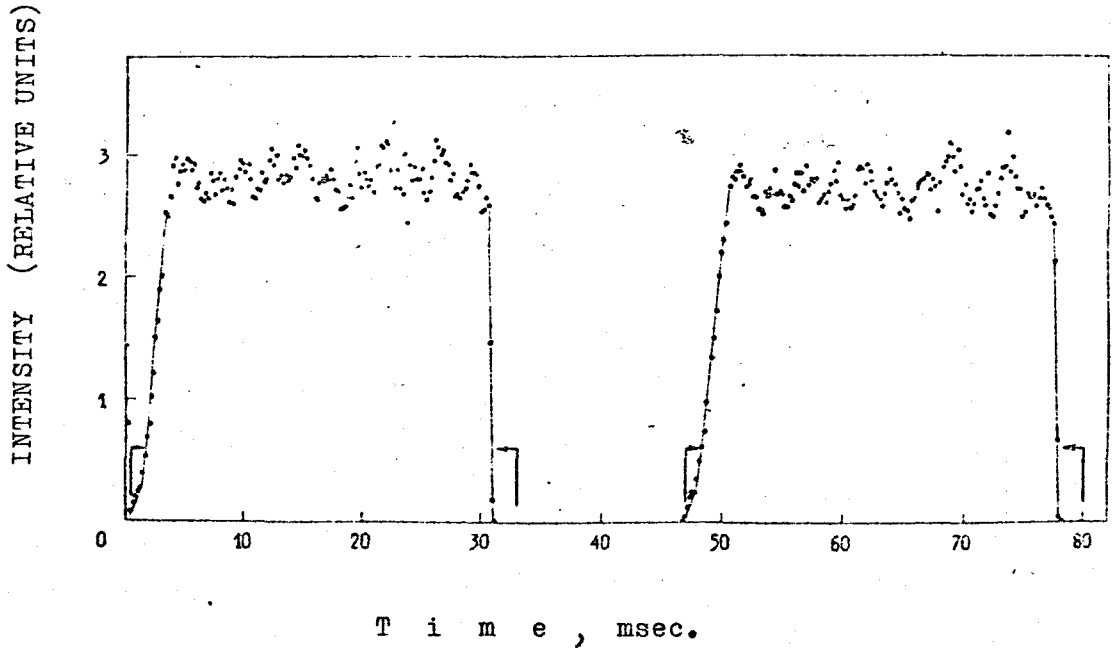

Fig. 8. Time structure of the proton beam at proton energies of 510, 650, 700 and 750 MeV.
Extension of the beam in time is performed by means of an Si electrode at an accelerator frequency of 20 Hz. The intensity of the internal beam was reduced 10-50 times by lowering a dummy target at 100 cm radius.
The arrows mark the window selected.
The beam intensity $I_p = 1.4 \cdot 10^4$ protons/sec.

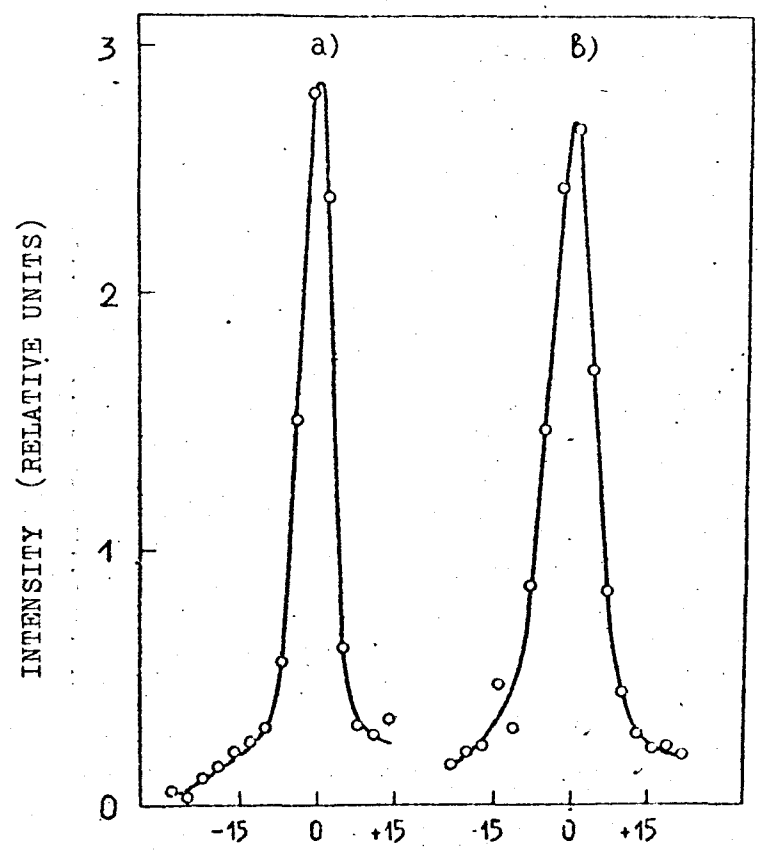

Fig. 9. Beam profile at input to ionization chamber. T_p = 510 MeV.

a) horizontal plane,
b) vertical plane.

Proportional chambers were used for the measurements.

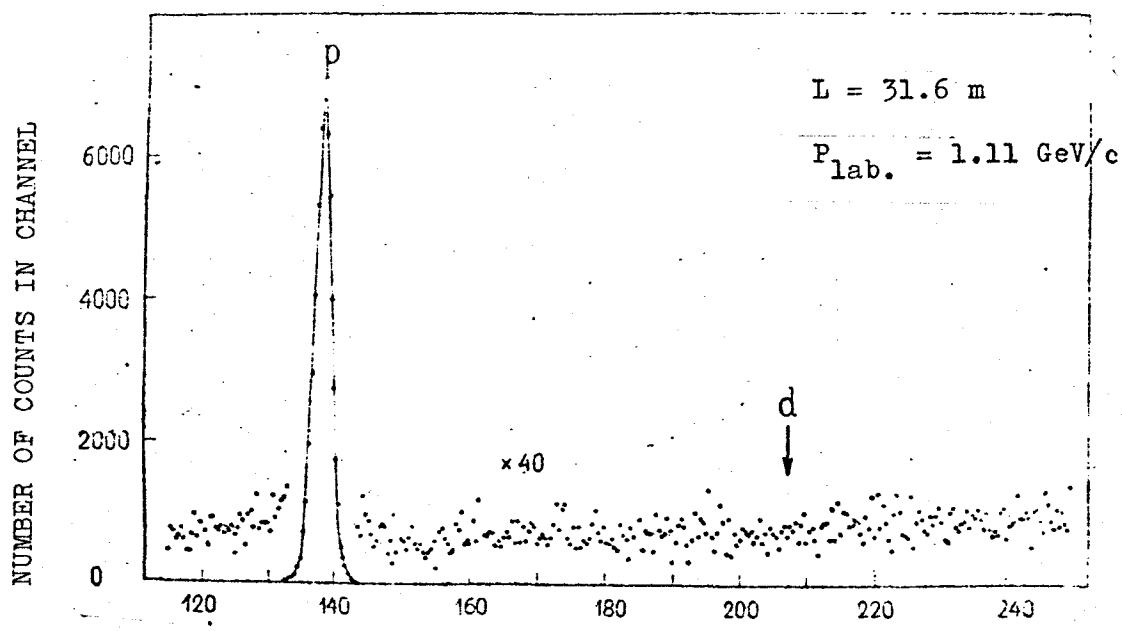

Fig. 10. Protons' time-of-flight spectrum at 510 MeV.
Path length - 31.6 m.
The arrow marks the expected position of the deuteron peak, corresponding to $P_{lab.}$ = 1.11 GeV/c.

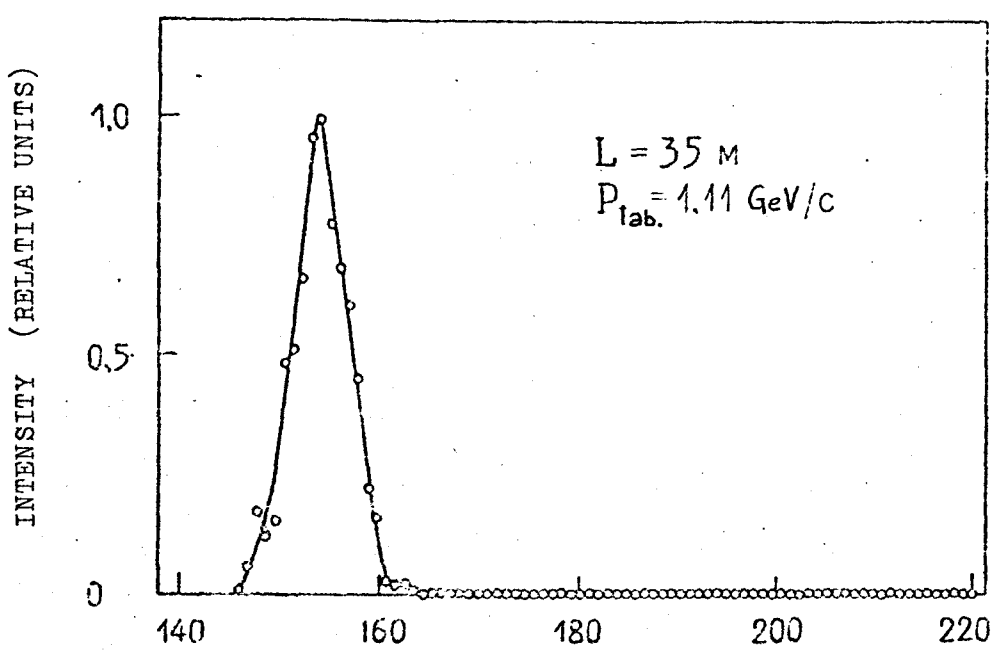

Fig. 11. Microstructure of proton beam.
In these measurements the start signal was a frequency mark from the HF generator and the stop signal was generated by a scintillation counter located 35 m from the attenuator.

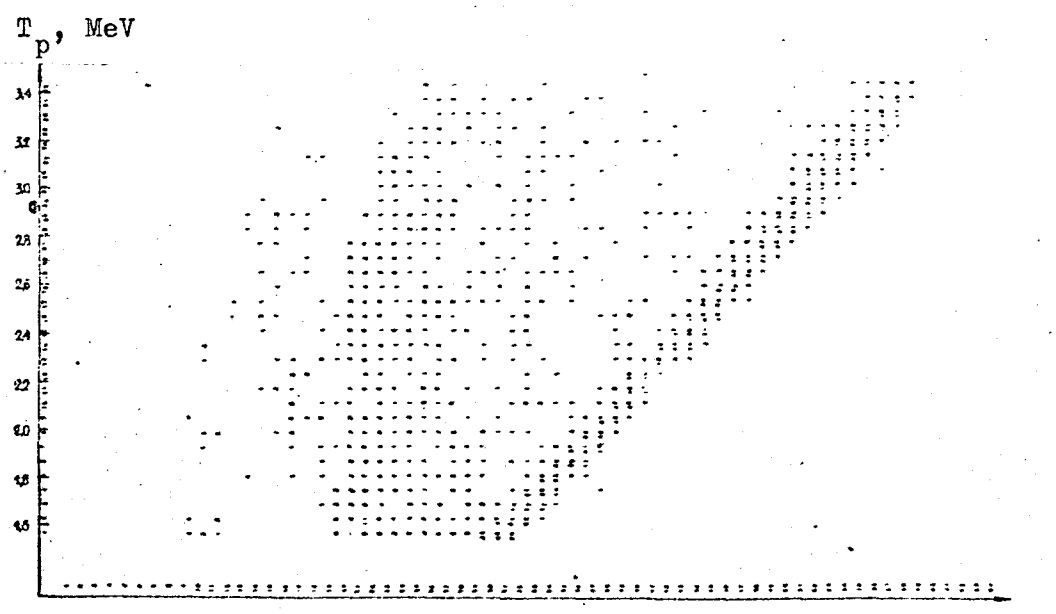

Fig. 12. Check matrix of events in the coordinates energy/ amplitude in angular channel.
Elastic events are grouped near the diagonal. On the left is the background caused by nuclear reactions and scattering of neutrons on hydrogen.

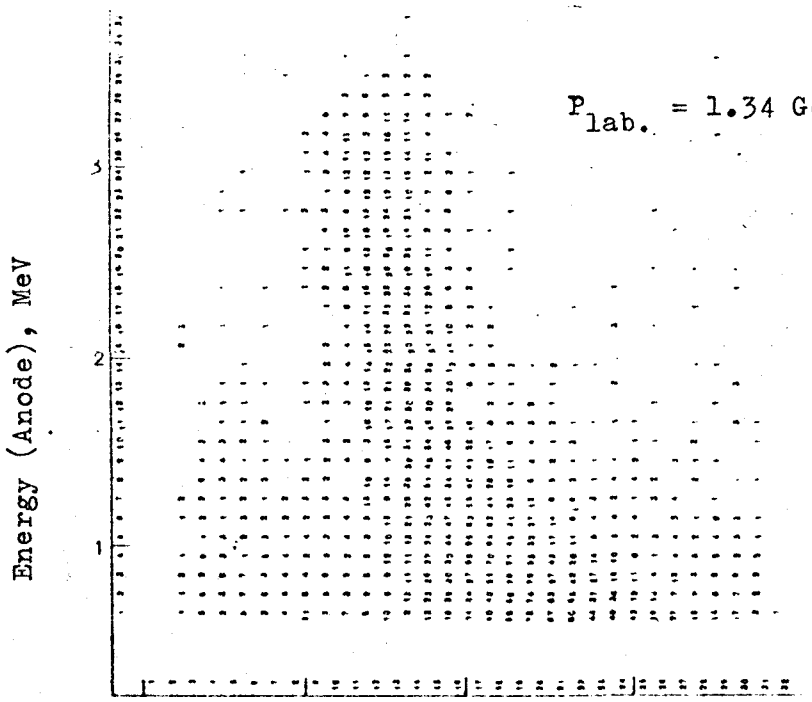

Fig. 13. Distribution of events in time window.

t_o - instant of traversal of proton,

t_k - instant of appearance of pulse at the chamber's cathode.

Measurements carried out at $P_{lab.}$ = 1.34 GeV/c.

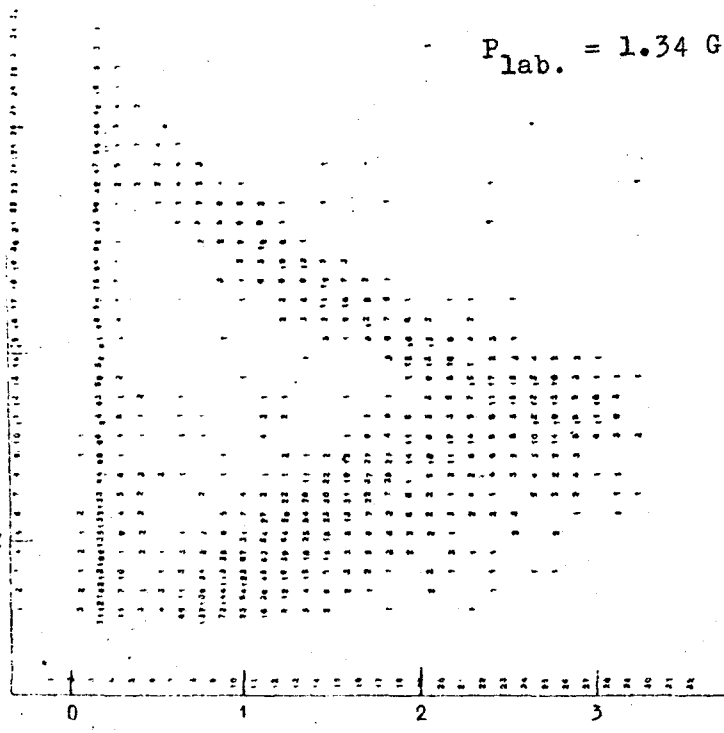

Fig. 14. Matrix of events in the coordinates pulse height at central anode/pulse height at orifice.
Measurements carried out at $P_{lab.}$ = 1.34 GeV/c.

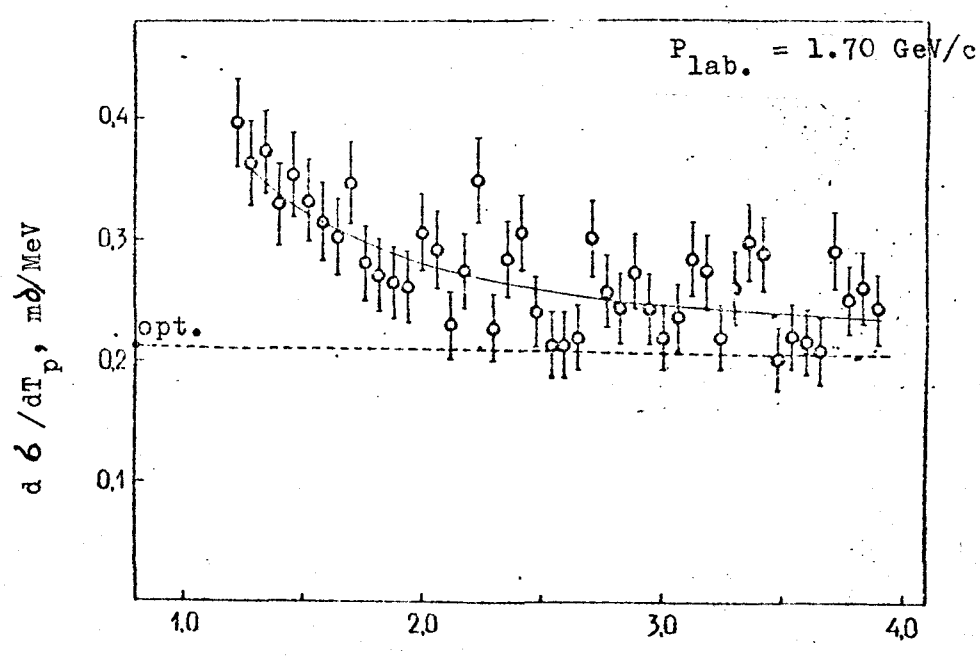

Fig. 15. Differential cross-section of elastic pp-scattering at $P_{lab.}$ = 1.70 GeV/c.
The solid line indicates the result obtained from the calculation in terms of the interference formula with parameters determined by the least squares method and given in Table 2.
The dotted line is where

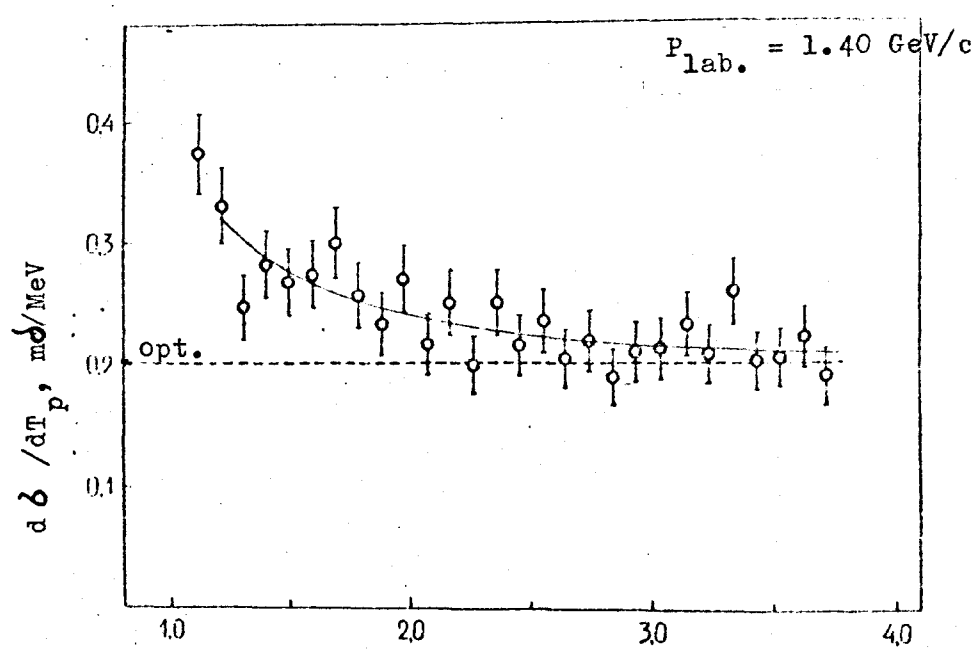

Fig. 16. Differential cross-section of elastic pp-scattering at $P_{lab.}$ = 1.40 GeV/c.

The solid line indicates the calculation in terms of the interference formula with parameters given in Table 2.
The dotted line is

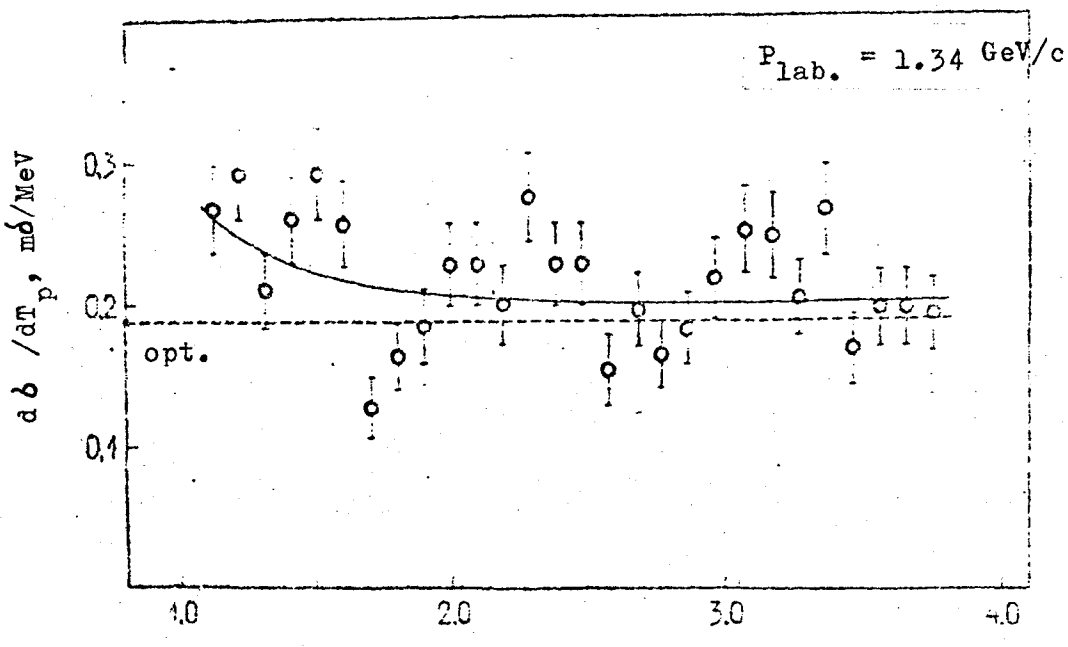

Fig. 17. Differential cross-section of elastic pp-scattering at $P_{lab.}$ = 1.34 GeV/c.
The solid line is the calculation in terms of the interference formula with parameters given in Table 2.
The dotted line is

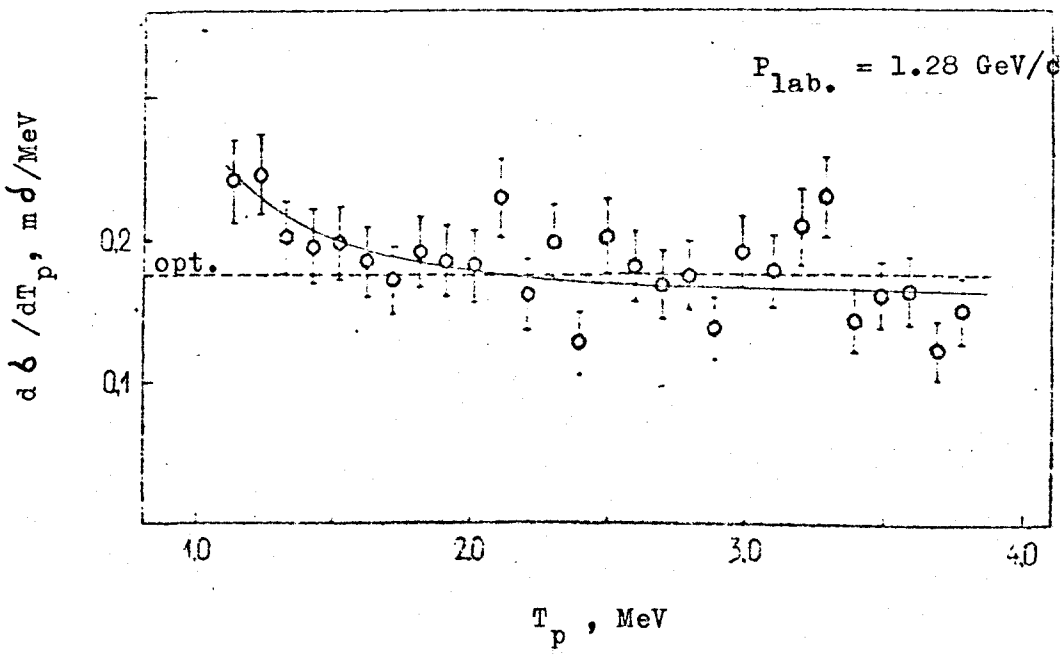

Fig. 18. Differential cross-section of elastic pp-scattering at $P_{lab.}$ = 1.28 GeV/c.
The solid line is the calculation in terms of the interference formula with parameters given in Table 2.
The dotted line is

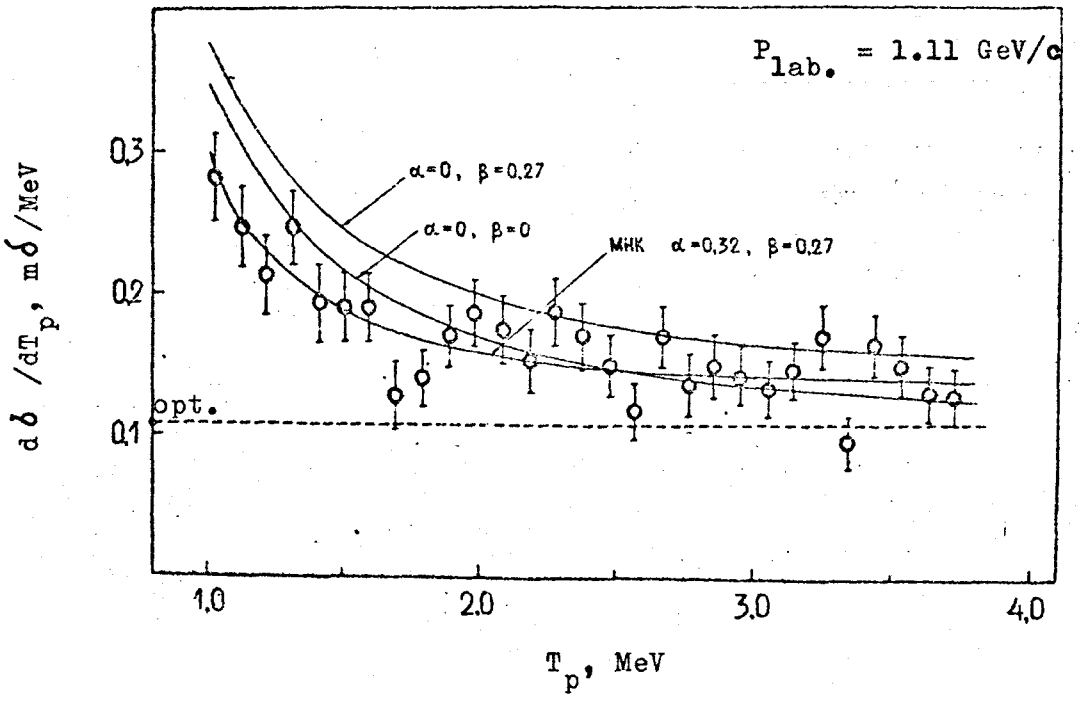

Fig. 19. Differential cross-section of elastic pp-scattering at $P_{lab.}$ = 1.11 GeV/c.
The solid line indicates the result obtained from the calculation in terms of the interference formula with different values for parameters α and β.
The dotted line is

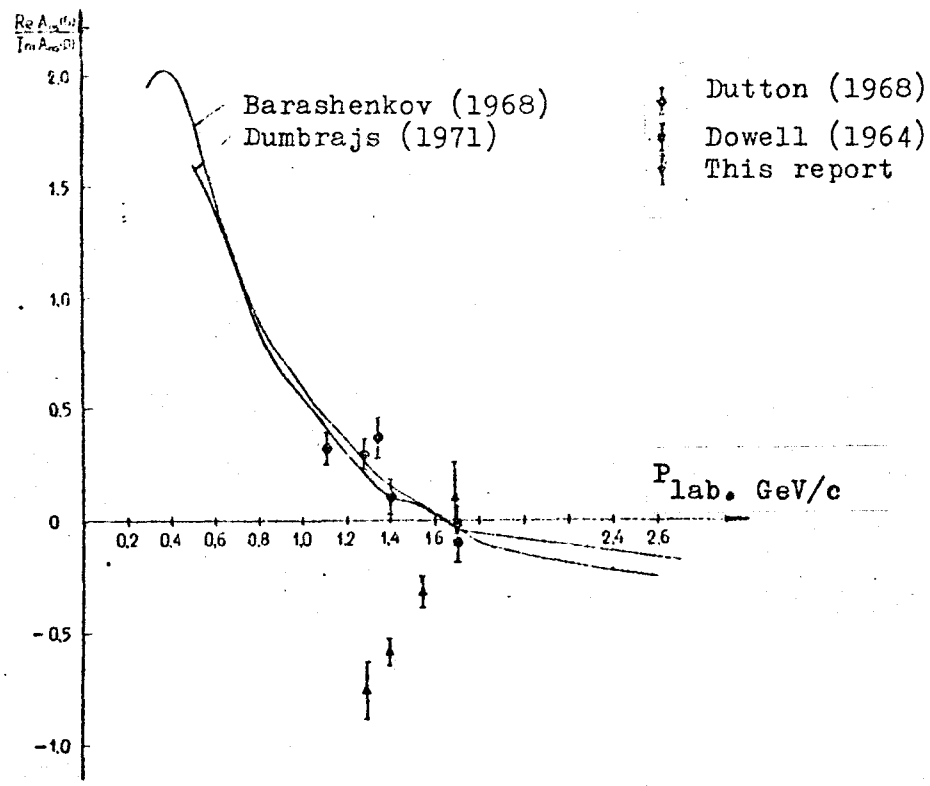

Fig. 20. Dependence on proton energy of the ratio of the real part of the spin-independent amplitude of pp-scattering to the imaginary part. The solid lines mark the results of calculations /9,10/ using dispersion relations. The figure includes the experimental results obtained by Dutton et al. /2/ and Dowell et al. /8/.